ELSEVIER

Polymer 43 (2002) 3257–3266

polymer

www.elsevier.com/locate/polymer

Swelling behavior of ordered miktoarm star block copolymer–homopolymer blends

Apostolos Avgeropoulos[a,b], Benita J. Dair[b], Edwin L. Thomas[b,*], Nikos Hadjichristidis[a,*]

[a]*Industrial Chemistry Laboratory, Department of Chemistry, University of Athens, Panepistimiopolis, Zografou, 15771 Athens, Greece*
[b]*Department of Materials Science and Engineering, Massachusetts Institute of Technology, 77 Massachusetts Avenue, Cambridge, MA 02139, USA*

Received 25 January 2002; received in revised form 25 January 2002; accepted 31 January 2002

Abstract

We report the morphological characterization of asymmetric miktoarm star block copolymers of the (PS-*b*-PI)$_n$PS type where $n = 2, 3$ (denoted 2DB and 3DB miktoarm stars, respectively) and a symmetric super H-shaped block copolymer of the (PS-*b*-PI)$_3$PS(PI-*b*-PS)$_3$ type (denoted SH) which were synthesized by anionic polymerization. The initial volume fraction of PS (ϕ_{PS}) for each copolymer was 0.51–0.56, giving a lamellar morphology. Addition of homopolystyrene (hPS) with a molecular weight lower than the respective PS blocks in the neat materials lead to a transition from the lamellar structure to hexagonally packed cylinders. Addition of low molecular weight homopolyisoprene (hPI) on the other hand, only resulted in swollen lamellae even when the overall composition was highly asymmetric (80/20). Changes in the lamellar spacing as well as in the respective PS and PI layer thickness were measured by SAXS. The transition from lamellae to cylinders with increased PS content occurred without the observation of an intervening cubic morphology for the 2DB and 3DB miktoarm stars. However, blends with 30 and 35% hPS ($(\phi_{PS})_{total} = 0.68$–$0.70$) with the super H-shaped block copolymer lead to the observation of lamellar-catenoid structures.

Keywords: Miktoarm star block copolymers; Binary blends; Morphological transition

1. Introduction

Early work on blends of diblock copolymers (AB) and homopolymer (hA), focused in both homopolymer solubility [1–3] and mechanical properties [4–8]. Morphologies of ordered and disordered spherical micelles were studied in well-defined binary blend systems [9–13]. When the added homopolymer molecular weight is comparable or smaller to the molecular weight of the matching block of the copolymer and the block copolymer content is sufficiently large, ordered microdomain morphologies are observed [7–13]: alternating lamellae, hexagonally close packed cylinders and ordered spheres on a cubic lattice, just as occurs for neat diblocks. Systematic examination of a series of blends of a neat lamellar poly(styrene-*b*-isoprene) diblock copolymer and various homopolymers showed that a fourth type of ordered microdomain morphology can also occur (a tricontinuous cubic morphology, either double diamond or more likely double gyroid, observed at a composition between the cylinders and lamellae) [14]. The effect of homopolymer concentration and homopolymer molecular weight on the equilibrium microdomain morphology, on the mean curvature of the PS–PI interface on the average interfacial area per copolymer junction were extensively studied [14].

A mean field theory derived by Milner [15,16] predicts the morphological behavior of A_nB_m-type miktoarm star block copolymers having various architectures including A_2B [17–20], A_3B [21], A_5B [22], A_nB_n stars [23–25] as well as multigraft blocks [26–28]. The compositional shift in the various microdomain regimes in the case of the A_2B stars compared to that of the AB diblocks is significant and increases even more for the A_3B stars. For example, in the case of A_3B stars [21], at a volume fraction of 0.56, the system exhibited a cylindrical microdomain morphology in good agreement with theory.

A double diamond cubic structure has been observed for the case of inverse miktoarm star block copolymers of the type $(PS_{\alpha M} - PI_M)_n - (PS_M - PI_{\alpha M})_n$, where $M \sim 20000$, $n = 2$ and the arm asymmetry parameter $\alpha = 4$ (α is the ratio of the outer block molecular weight to that of the inner block) [29]. The volume fraction of the PS component is approximately 0.5 and the copolymer has 1 central and 4

* Corresponding authors. Tel.: +1-617-253-6901; fax: +1-617-258-6135 (E.L. Thomas).
Tel.: +3-01-727-4330; fax: +3-01-722-1800. (N. Hadjichristidis).
E-mail addresses: elt@mit.edu (E.L. Thomas), hadjichristids@chem.uoa.gr (N. Hadjichristidis).

0032-3861/02/$ - see front matter
PII: S0032-3861(02)00131-3

peripheral junctions. The formation of a tricontinuous cubic microdomain structure in this compositionally symmetric system arises in order to relieve the overcrowding of the four peripheral PS-*b*-PI junctions by providing a curved intermaterial dividing surface (IMDS) with a triply periodic microdomain structure, relieving chain stretching by allowing some bridge conformations to the interior blocks of the miktoarm stars.

The present work examines the influence of architecture at constant overall copolymer composition on microdomain structure as well as investigates how the incorporation of homopolymers into miktoarm star block and super H-shaped block copolymers influences the morphology. A schematic of the three neat copolymers used for this study is shown in Fig. 1. There are two star blocks, with two (2DB) or three (3DB) diblock arms and a single homopolymer arm. The super H-shaped block copolymer is essentially a coupled pair of the (PS-*b*-PI)$_3$PS miktoarm stars. As is evident from Fig. 1, the miktoarm stars and the super H-shaped block copolymers can be considered as a combination of triblocks and diblocks.

The samples examined are designated as follows: the 3-miktoarm star of (PS-*b*-PI)$_2$PS is sample 2DB-16/16, the 4-miktoarm star of (PS-*b*-PI)$_3$PS is sample 3DB-20/20, and the super H-shaped block copolymer of ((PS-*b*-PI)$_3$PS(PI-*b*-PS)$_3$ is sample SH-20/20. The molecular weights of PS and PI blocks were approximately equal, except that of the PS difunctional macroanion in the super H copolymer is approximately twice that of the monofunctional PS blocks. All the neat copolymers have their composition very close to 50/50 and all form lamellar microdomain structures. Binary blends of these copolymers with hPS or hPI, allows investigation of the swelling behavior of the lamellar phase with variation of the appropriate total PS and PI volume fraction and to explore for possible order–order transitions. In particular, by making blends with each type of homopolymer, one can investigate how the addition of hPS would affect the exterior PS end blocks (only in the SH-20/20 sample is there an interior PS chain terminated by two junction points) and how the addition of the hPI would influence the ratio of bridges to loops in the interior PI blocks.

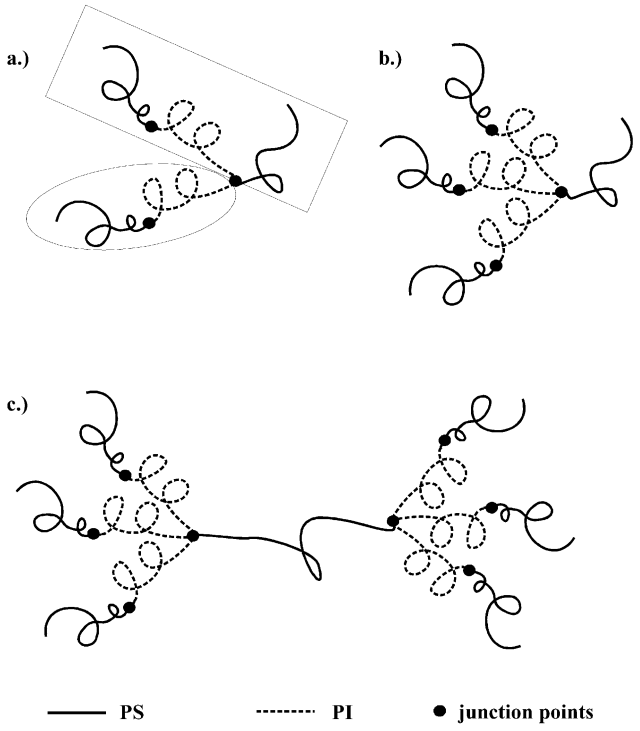

Fig. 1. Schematic presentation of the block copolymers studied. (a) 3-Miktoarm star block copolymer of the (PS-*b*-PI)$_2$PS type. The scheme shows that the polymer can be considered as a combination of a diblock (ellipse) and a triblock (rectangle). (b) 4-Miktoarm star block copolymer of the (PS-*b*-PI)$_3$PS type. It can be considered as a combination of 2 diblocks and a triblock. (c) Super H-shaped block copolymer of the (PS-*b*-PI)$_3$PS(PI-*b*-PS)$_3$ type.

2. Experimental section

The miktoarm star block copolymers and the super H-shaped block copolymers used for this study were prepared by combining anionic polymerization and high vacuum techniques. The reactions and the processes used are described in detail elsewhere [30]. The molecular characteristics for the copolymers are given in Table 1. The characterization methods used were size exclusion chromatography (SEC), membrane osmometry (MO), low-angle laser light scattering (LALLS), ^{1}H NMR and UV. The last two methods were used to determine the microstructure of the PI and the volume fraction of PS, respectively. The polyisoprene block has an approximate microstructure distribution of 70% *cis*-1,4, 24% *trans*-1,4 and 6% 3,4 addition as determined by ^{1}H NMR. The glass transition temperature of the polystyrene component was measured to be 101, 99.5, and 102 °C, respectively for the samples 2DB-16/16, 3DB-20/20 and SH-20/20, on a TA Instruments 2910 DSC/Modulated DSC. Possible polymer degradation after the annealing procedures was checked by dissolving a portion of the annealed samples in THF and re-running SEC. No detectable difference was observed, indicating no high temperature branching of PI. Calculated values of χN are given for $T = 120$ °C along with theoretical values for the spinodal temperature for each of the neat copolymers [31] in Table 1.

The homopolymers (hPS and hPI) were purchased from Pressure Chemical Co. The weight-average molecular weights and the polydispersity indices are 10,200–13,000 and 1.06–1.08 g/mol, respectively.

The casting protocol for blend preparation was designed to reproducibly prepare bulk binary blends at thermodynamic equilibrium by solvent casting and annealing, the same preparation as that used for the neat copolymers. For SAXS and TEM characterization, approximately 0.7 mm thick films of the materials and the binary blends were cast

Table 1
Molecular and morphological characteristics of the miktoarm star and super H-shaped block copolymers

Sample	$\bar{M}_n$ (MO) ($\times 10^{-3}$ g/mol)	$\bar{M}_w$ (LALLS) ($\times 10^{-3}$ g/mol)	I (SEC)	ϕ_{PS}	d_{001} (Å)	$(\chi N_O)_S$ [a]	$\chi N_{(120\,^\circ C)}$ [b]	σ/chain (Å^2)	$\sigma_{average}$/junction (Å^2)
2DB-16/16	78.2	82.1	1.04	0.56	206	11.7	67	1284	428
3DB-20/20	126.0	132.8	1.05	0.51	254	10.3	119	1780	445
SH-20/20	266.0	282.0	1.07	0.55	265	9.5	248	3546	443
PS/PB$_{(20.5/20.5\ K)}$ [c]	41.0	–	1.07	0.50	387	10.5	27	380	380
PS/PI/PS$_{(20/30/20)}$	72.1	76.5	1.06	0.54	278	17.1	63	886	443

[a] From Ref. [31].
[b] $\chi_{SI}(120\,^\circ C) = 0.074$ (from Ref. [44]).
[c] $\chi_{SB}(120\,^\circ C) = 0.047$ (from Ref. [45]).

from a dilute solution (~4 wt%) in a nearly nonselective solvent (toluene) over a period of 1 week at ambient conditions. The films were then dried under vacuum for 3 days at room temperature and finally annealed at 120 °C for 1 week under vacuum. For TEM investigation, approximately 50 nm thick sections of the block copolymers were cryomicrotomed at −110 °C using a Reichert–Jung FC 4E cryoultramicrotome equipped with a diamond knife. To increase the mass-thickness contrast, the thin sections were exposed to OsO_4 vapors for 2 h. The stained sections were examined in a JEOL 200CX electron microscope operated at 200 kV in the bright field mode.

The X-ray diffraction (SAXS) data were acquired at the time-resolved diffraction facility (station X12B) at the National Synchrotron Light Source at Brookhaven National Laboratory (BNL) using a custom-built two-dimensional detector (10 × 10 cm, 512 × 512 pixels). The optical system provides a doubly-focused (spot size, 0.5 × 0.5 mm fwhm) monochromatic X-ray beam (bandpass, $\sim 5 \times 10^{-4}$ $\Delta\lambda/\lambda$ with a wavelength of $\lambda = 1.54$ Å.

3. Results

3.1. Neat miktoarm stars

The results from TEM and SAXS for the two neat miktoarm star and super-H block copolymers are given in Fig. 2a and b, respectively. The TEM pictures show that despite the various complex architectures all samples are

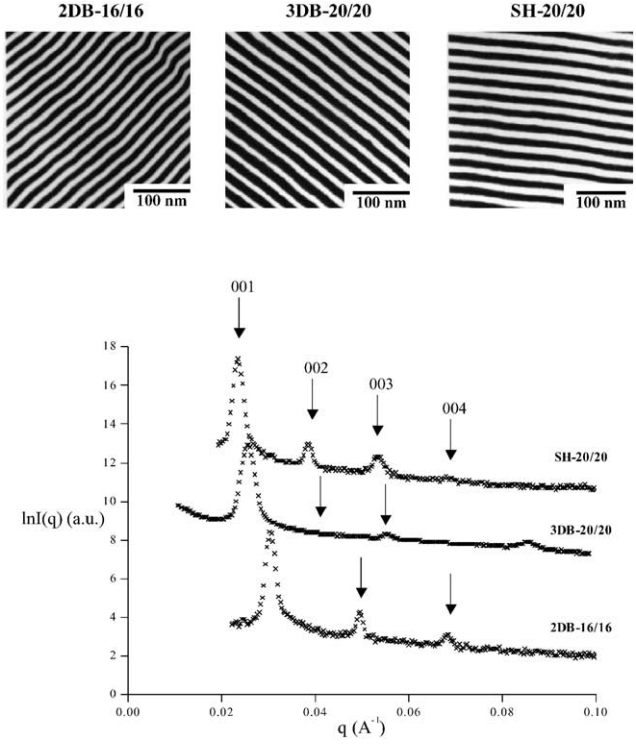

Fig. 2. TEM images and SAXS plots of ln $I(q)$ vs. q for the three neat samples, all exhibiting a lamellar morphology.

lamellar. The SAXS peaks in all samples correspond to q_n/q_1 ratios approximately equal to 1:2:3, characteristic for the lamellar morphology. The existence of third order peaks in the SAXS patterns shows that the samples are well-ordered and well microphase separated. The d_{001}-spacing (Table 1) increases from the 2DB-16/16 star block copolymer to the 3DB-20/20 copolymer. The 40 K PS midblock of the super H-shaped block copolymer leads to a modest increase (4%) of the lamellar period over that of the 3DB-20/20 copolymer.

As is evident, the different molecular architectures did not alter the usual lamellar microdomain morphology which occurs at approximately 50/50 composition, suggesting that a mixture of loop and bridge conformations of the PI blocks onto a single flat IMDS is more favorable than the molecular conformation in which two differently curved IMDS are formed and all interior blocks form bridges.

The 3-miktoarm star block has an architecture similar to A_2B miktoarm stars but the A arms are comprised of a diblock instead of a single block leading to increased number of junctions for the molecule (3 in this particular case). The average area of interface per copolymer chain, which is a measure of the average separation of the copolymer junctions, reflects the nature of packing environment and the conformation of PS and PI blocks. The average area per copolymer is the area of the PS–PI interface divided by the number of copolymer molecules on the PS–PI interface. The area of the IMDS per simple diblock molecule for a lamellar structure of repeat spacing d_{001} is given by the equation:

$$\sigma_i = \frac{2M_i}{d_{001}\rho_i N_{Av}\phi_i} \tag{1}$$

where N_{Av} is Avogadro's number, M_i is the total molecular weight of the i type blocks, ρ_i is the density of component i (1.01 g/cm^3 for PS and 0.864 g/cm^3 for PI) [32] and ϕ_i is the volume fraction. The densities used are characteristic for 120 °C, the annealing temperature of all samples. If ambient temperature densities were used (1.06 g/cm^3 for PS and 0.913 g/cm^3 for PI) the change in the total volume fraction of each component is less than 1.5 vol%. The average area per junction can be approximated by dividing σ_i by the number of junctions per chain. The results are shown in Table 1 together with the molecular characteristics of the polymers. Also shown in Table 1, for comparison reasons are the lamellar repeat, area per chain and area per junction for a diblock (PS/PB) and a triblock (PS/PI/PS) copolymer. The area per junction for the architecturally complex copolymers is seen to be very close to that calculated to corresponding simple diblock and triblocks of comparable composition and block molecular weight. It is also possible to calculate the preferred interfacial area per junction for a miktoarm star assuming that the interior junctions and the exterior junctions lay on separate IMDS. The exterior junction is like that of a simple diblock whereas the interior junction with its higher junction functionality desires an increase in the interfacial area by a factor:

$$p_s \frac{d_d}{d_s}\frac{\phi_d}{\phi_s} \tag{2}$$

where p_s is the number of arms, d_d and d_s are the lamellar period in the diblock and in the star, respectively, and ϕ_d and ϕ_s are the respective volume fractions. If the preferred interfacial areas of the exterior and interior junctions are sufficiently different, a morphology which has a variation of the interfacial curvature over the IMDS (such as double gyroid or double diamond) or perhaps a structure comprised two differently curved IMDS (such as core-shell cylinders) may result.

The area per chain for the binary blends exhibiting hexagonally packed cylindrical morphologies can be calculated from:

$$\sigma_i = \frac{2M_i}{d_{10\bar{1}0}\rho_i N_{Av}}\left(\frac{\pi}{\frac{\sqrt{3}}{2}\phi_i}\right)^{1/2} \tag{3}$$

where d is the $(10\bar{1}0)$ spacing of the hexagonally packed cylinders and M_i and ϕ_i correspond to the volume fraction of the minority (cylinder forming) block. Homopolymers mix with their respective blocks and the layer thicknesses reflect the axial changes perpendicular to the PS–PI interface due to the swelling by the homopolymer. The individual polystyrene and polyisoprene layer thicknesses l_{PS} and l_{PI}, respectively (for the lamellar samples) are given by: $l_i = \phi_i d_{001}$.

The layer thickness for PS and PI for all of the lamellar samples are shown in Table 3 and plots of the lamellar period and the respective layer thickness are shown in Fig. 6. Mixing between homopolymer and the respective blocks near the PS/PI interfaces increases the layer thickness. The distribution of the homopolymer across the block layer depends on the loss of entropy of the homopolymer near the interface versus the induced relaxation of block stretching by lateral swelling. Due to the lateral swelling of one layer by the homopolymer, the thickness of the other block layer decreases. It is quite remarkable to note that for the addition of hPI the morphological behavior of the final material is lamellar even to very low PS volume fractions (0.20).

3.2. Homopolymer–miktoarm star block copolymer blends

It is of interest to explore how the addition of homopolymer can influence the morphology of the miktoarm star block copolymers. The location of the block, interior vs. exterior, influences the nature of the swelling of its domain by the homopolymer, and therefore blends were made with both homopolystyrene and homopolyisoprene. A total of six families of blends were made: 2DB-16/16 with 5–40% hPS; 2DB-16/16 with 5–60% hPI; 3DB-20/20 with 10–60% hPS; 3DB-20/20 with 5–60% hPI; SH-20/20 with

Table 2
Results from TEM[a] and SAXS[b] for the neat block copolymers and hPS or hPI binary copolymer blends. Area per chain for the LC sample[c] by using Eq. (1) for simple lamellar structure. About 10%[d] cubic phase estimated from TEM images

Sample	hPS (wt%)	hPI (wt%)	$(\phi_{PS})_{tot}$	Morphology[a]	d_1 (Å)[b]	σ/chain (Å^2)	σ/junction (Å^2)
2DB-16/16	0	–	0.56	Lamellae	206	1303	434
2DB-16/16	5	–	0.58	Lamellae	213	1220	407
2DB-16/16	10	–	0.60	Lamellae	218	1251	417
2DB-16/16	20	–	0.65	Lamellae	232	1344	448
2DB-16/16	30	–	0.69	Lamellae	233	1496	499
2DB-16/16	32	–	0.70	Lamellae	234	1630	543
2DB-16/16	34	–	0.71	Cylinders	234	1649	550
2DB-16/16	36	–	0.72	Cylinders	237	1657	552
2DB-16/16	38	–	0.73	Cylinders	240	1666	555
2DB-16/16	40	–	0.74	Cylinders	246	1656	553
2DB-16/16	–	5	0.53	Lamellae	207	1370	457
2DB-16/16	–	10	0.50	Lamellae	210	1432	477
2DB-16/16	–	20	0.44	Lamellae	212	1612	537
2DB-16/16	–	40	0.33	Lamellae	213	2139	713
2DB-16/16	–	45	0.30	Lamellae	213	2353	784
2DB-16/16	–	50	0.27	Lamellae	217	2566	855
2DB-16/16	–	55	0.24	Lamellae	220	2778	926
2DB-16/16	–	60	0.22	Lamellae	224	2896	965
3DB-20/20	0	–	0.51	Lamellae	254	1838	460
3DB-20/20	10	–	0.56	Lamellae	273	1816	454
3DB-20/20	20	–	0.61	Lamellae	289	1936	484
3DB-20/20	30	–	0.65	Lamellae	298	1948	487
3DB-20/20	35	–	0.68	Lamellae	301	2266	567
3DB-20/20	40	–	0.70	Cylinders	302	2512	628
3DB-20/20	45	–	0.72	Cylinders	306	2566	641
3DB-20/20	50	–	0.75	Cylinders	325	2557	639
3DB-20/20	60	–	0.78	Cylinders	360	2581	645
3DB-20/20	–	5	0.48	Lamellae	259	1915	479
3DB-20/20	–	10	0.46	Lamellae	265	1996	499
3DB-20/20	–	20	0.40	Lamellae	267	2229	557
3DB-20/20	–	40	0.30	Lamellae	268	2960	740
3DB-20/20	–	45	0.27	Lamellae	270	3266	817
3DB-20/20	–	50	0.25	Lamellae	262	3635	909
3DB-20/20	–	55	0.22	Lamellae	272	3979	995
3DB-20/20	–	60	0.20	Lamellae	269	4425	1106
SH-20/20	0	–	0.55	Lamellae	265	3546	443
SH-20/20	20	–	0.64	Lamellae	296	4095	512
SH-20/20	25	–	0.66	Lamellae	305	4209	526
SH-20/20	30	–	0.68	Lamellar caten[c]	299	4561	570
SH-20/20	35	–	0.70	Lamellar caten[c]	306	4754	594
SH-20/20	40	–	0.73	Cylinders	296	5403	675
SH-20/20	–	5	0.52	Lamellae	263	3780	473
SH-20/20	–	10	0.49	Lamellae	272	3872	485
SH-20/20	–	20	0.43	Lamellae	274	4387	548
SH-20/20	–	40	0.32	Lamellae + cub[d]	275	5874	734
SH-20/20	–	45	0.29	Lamellae	274	6505	813
SH-20/20	–	50	0.26	Lamellae	276	7203	900

20–50% hPS and SH-20/20 with 5–40% hPI. Table 2 lists the morphology and domain spacings as well as the average area per chain and average area per junction for all six families of blends comprising 47 individual samples (including the three neat materials).

The homopolymer mixes with the respective block and swells its domain both axially and laterally as evidenced by an increase in the layer spacing of the swollen block, an increase of σ_i [33] and a decrease in the layer spacing of the other block (Tables 2 and 3). At sufficiently large homopolystyrene content, order–order transitions (i.e. lamellar to cylinders) occur. Surprisingly, even at very high homopolyisoprene content (up to 80% PI) the asymmetric structure comprised of a thick PI layer and a thin PS layer remains lamellar while the total lamellar repeat period is nearly constant.

3.2.1. DB-20/20 Blends

We now report the results for the blends of each of the copolymer architectures with hPI and hPS. Despite

Table 3
Polystyrene (l_{PS}) and polyisoprene (l_{PI}) layer thicknesses for the neat materials and the binary blends

Sample	hPS (wt%)	hPI (wt%)	l_{PS} (Å)	l_{PI} (Å)	hPS Swelling	hPI Swelling
2DB-16/16	0	–	115	91	$dl_{PS}/d\phi_{PS} = 348$	$dl_{PS}/d\phi_{PI} = -210$
2DB-16/16	5	–	123	90		
2DB-16/16	10	–	131	87		
2DB-16/16	20	–	151	81		
2DB-16/16	30	–	161	72		
2DB-16/16	32	–	164	70		
2DB-16/16	–	5	110	97	$dl_{PS}/d\phi_{PS} = -147$	$dl_{PS}/d\phi_{PI} = 239$
2DB-16/16	–	10	105	105		
2DB-16/16	–	20	93	119		
2DB-16/16	–	40	70	143		
2DB-16/16	–	45	64	149		
2DB-16/16	–	50	59	158		
2DB-16/16	–	55	53	167		
2DB-16/16	–	60	49	175		
3DB-20/20	0	–	129	125	$dl_{PS}/d\phi_{PS} = 446$	$dl_{PS}/d\phi_{PI} = -255$
3DB-20/20	10	–	153	120		
3DB-20/20	20	–	176	113		
3DB-20/20	30	–	194	104		
3DB-20/20	35	–	205	96		
3DB-20/20	–	5	124	135	$dl_{PS}/d\phi_{PS} = -165$	$dl_{PS}/d\phi_{PI} = 283$
3DB-20/20	–	10	122	143		
3DB-20/20	–	20	107	160		
3DB-20/20	–	40	80	188		
3DB-20/20	–	45	73	197		
3DB-20/20	–	50	66	196		
3DB-20/20	–	55	60	212		
3DB-20/20	–	60	54	215		
SH-20/20	0	–	146	119	$dl_{PS}/d\phi_{PS} = 457$	$dl_{PS}/d\phi_{PI} = -255$
SH-20/20	20	–	189	107		
SH-20/20	25	–	201	104		
SH-20/20	30	–	203	96		
SH-20/20	35	–	214	92		
SH-20/20	–	5	137	126	$dl_{PS}/d\phi_{PS} = -179$	$dl_{PS}/d\phi_{PI} = 293$
SH-20/20	–	10	133	139		
SH-20/20	–	20	117	156		
SH-20/20	–	40	88	187		
SH-20/20	–	45	80	194		
SH-20/20	–	50	72	204		

increasing the total volume fraction of PS for the binary blends 3DB-20/20-hPS, from 0.51 to 0.56, 0.61, 0.65 and 0.68 by adding up to 35 wt% of hPS, the morphology remains lamellar. Increasing the volume fraction up to 0.70 by adding 40 wt% of hPS resulted to a transition from lamellae to hexagonally packed cylinders *without* the observation of a cubic microdomain structure. TEM images and SAXS patterns for some of these binary blends are shown in Figs. 3c, d and 5a, respectively. The corresponding d_{001} or $d_{10\bar{1}0}$-spacings for each type of first peak (for lamellae or cylinders) are given in Table 2, as d_1. TEM shows that the homopolymer was completely absorbed in the PS phase, since no separare pools of hPS were observed. By swelling the PS layers, it is evident from Table 2 that the PS layer thickness (l_{PS}) is increased and the l_{PI} is decreased making the formation of PI bridges easier and lessening any tendency to develop two types of IMDS.

In the case of 3DB-20/20-hPI blends it was observed that in blends containing 5–60% of hPI, which diminishes the total PS volume fraction from 0.48 to 0.20, the structure remains lamellar (Table 2). TEM images and SAXS patterns for some of these binary blends are shown in Figs. 4c, d and 5b, respectively. Again, no macrophase separation of the homopolymer is observed in the TEM images. Thus both homopolyisoprene and homopolystyrene blends with 3DB-20/20 occur without the observation of a cubic morphology, even at compositions where neat diblock and triblock copolymers or their blends with a homopolymer exhibit an double diamond or double gyroid structure [34–36] (Ref. [35] gives a review of the compositions of the bicontinuous cubic structures reported in the literature).

3.2.2. DB-16/16 blends

A more extensive experimental study was done for the 3-miktoarm star block copolymer (2DB-16/16) blends, in order to find precisely the composition where the added homopolymer induces a transition from the flat IMDS of lamellae. TEM images and SAXS patterns of some of the

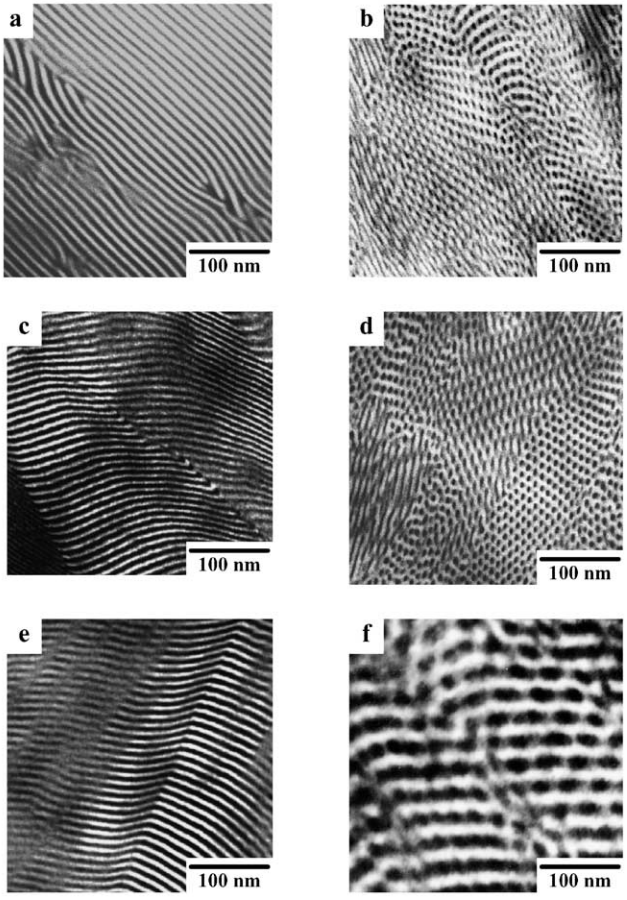

Fig. 3. TEM images for selective binary blends of the neat copolymers with hPS (a) 2DB-16/16 + 10 wt% hPS; (b) 2DB-16/16 + 40 wt% hPS; (c) 3DB-20/20 + 10 wt% hPS; (d) 3DB-20/20 + 40 wt% hPS; (e) SH-20/20 + 10 wt% hPS; (f) SH-20/20 + 35 wt% hPS (lower magnification TEM image to exhibit both structures).

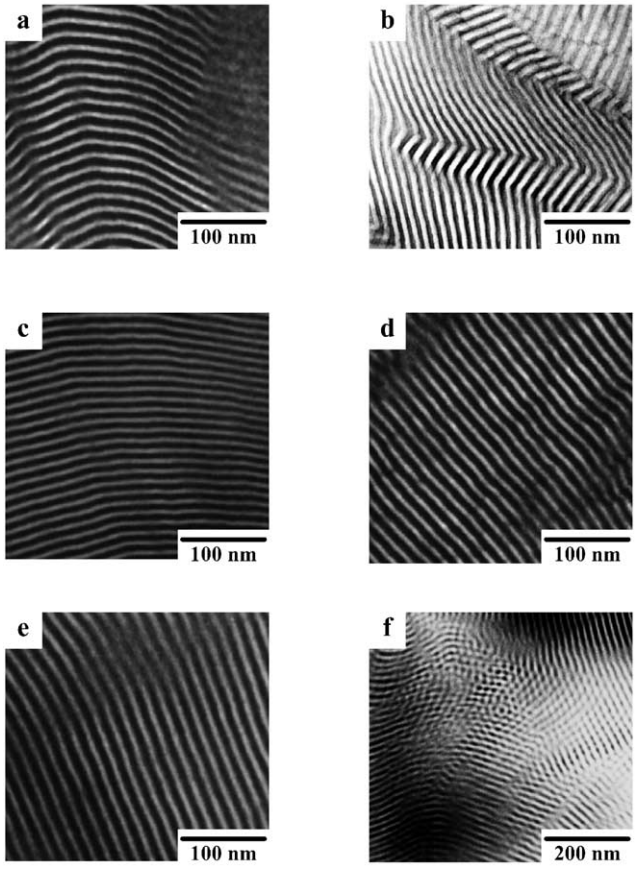

Fig. 4. TEM images for selective binary blends of the neat copolymers with hPI (a) 2DB-16/16 + 10 wt% hPI; (b) 2DB-16/16 + 40 wt% hPI; (c) 3DB-20/20 + 10 wt% hPI; (d) 3DB-20/20 + 40 wt% hPI; (e) SH-20/20 + 10 wt% hPI; (f) SH-20/20 + 40 wt% hPI.

samples are exhibited in Figs. 3a, b and 5a, respectively. The peaks resolved from SAXS correspond to a ratio of 1:2:3 for the five binary blends exhibiting a lamellar morphology and to a ratio of $1:\sqrt{3}:\sqrt{4}$ for the four samples exhibiting hexagonally packed cylinders. The corresponding hPI blends show similar behavior. The lamellar morphology is observed even when the total PS volume fraction is decreased to 0.22 by adding 60% of hPI. TEM images and SAXS plots for some of the hPI blends are shown in Figs. 4a, b and 5b, respectively. The results are summarized in Table 2. Again, as in the case of 3DB-20/20 blends with hPS, lamellae persist up to $\phi_{PS} = 0.70$, then at $\phi_{PS} = 0.71$ hexagonally packed cylinders appear *without* an intervening bicontinuous cubic phase. The transition occurs without even the appearance of a noticeable biphasic region.

3.2.3. SH-20/20 blends

In binary blends of hPS with the super H-shaped block copolymer (SH-20/20), the morphology remains lamellar up to volume fraction of PS equal to 0.66, as observed in the case of the binary blends of the 2DB and 3DB polymers. However, by increasing the PS volume fraction to 0.68, a transformation to the lamellar catenoid (LC) structure occurs. This structure appears similar to the LC structure that was previously found in binary blends of a PS-*b*-PB diblock and homopolymer (hPS) at a PS volume fraction range 0.65–0.67 [37]. A LC structure was first observed in thin films of a PS-*b*-PB diblock copolymer with a PS volume fraction of 0.46 in which both layers were penetrated by channels of the other component [38]. The LC phase is comprised of a tricontinuous PS domain, with the layers of the minority PB component penetrated by channels of PS. A similar structure has been observed in sodium dodecyl sulfate lipids [39] and assigned a three-dimensional rhombohedral space group.

Binary blends of hPI blends with the super H-shaped block copolymer sample were also prepared and the results are summarized in Table 2. When the total volume fraction of PS is decreased to 0.32 the morphology obtained is predominantly lamellar but about 10% of a coexisting cubic phase is detected by TEM. By tilting thin sections both 4-fold and 3-fold TEM images were obtained indicating some sort of tricontinuous cubic phase. The identification (by TEM) of a lamellar + cubic biphasic system in a

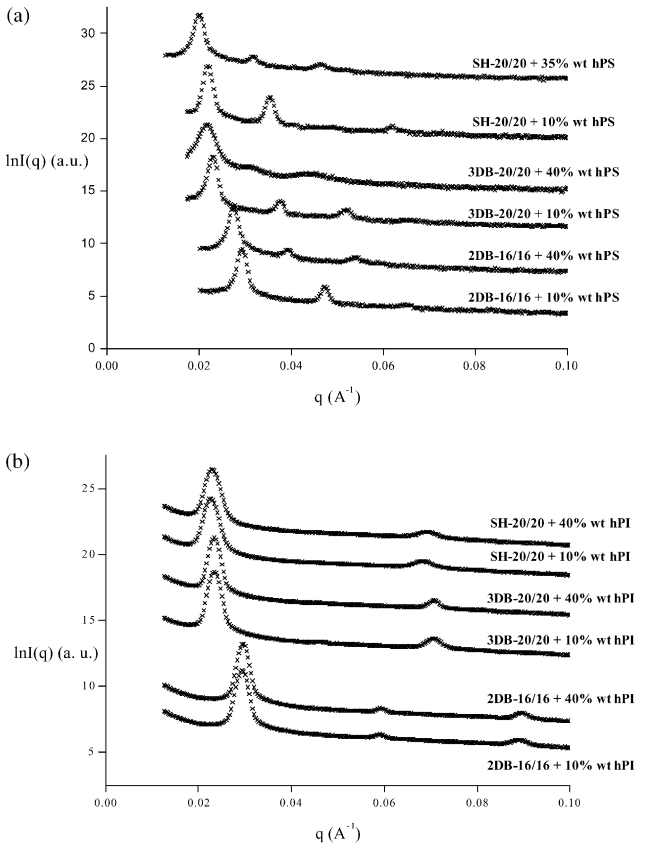

Fig. 5. SAXS plots of ln $I(q)$ vs. q for the samples exhibited in (a) Fig. 3 and (b) Fig. 4.

diblock–homopolymer blend has already been reported to the literature [34], but no explanation for this biphasic region was given [34]. TEM images and SAXS plots for a few of the SH-20/20 + hPI blends are exhibited in Figs. 4e, f and 5b, respectively.

4. Discussion

Tables 2 and 3 and Fig. 6a, c show that adding hPS increases the repeat spacing for the blends at a much higher rate compared to the very modest increase of the spacing when adding hPI. Addition of hPS increases the PS layer thickness while decreasing that of the PI. The opposite trend occurs when swelling with hPI (Tables 2 and 3, Fig. 6b, d).

The area per junction (Table 2) and the respective layer thickness (Table 3) provide important information for understanding the swelling behavior of the various miktoarm star copolymers. The behavior is quite different when hPS is added compared to when hPI is added. The increase in the area per junction in both the 2DB and 3DB-hPS blends is relatively small (27–40%, respectively) whereas, in the 2DB-hPI the area per junction more than doubles and in the 3DB-hPI blends it nearly triples. This trend also holds for the SH blends. The PS swelling causes an increase in σ_i of about 50%, whereas the PI swelling increases σ_i by over 200%. The plots of the individual layer thickness l_{PS} and l_{PI} versus composition allows the calculation of the incremental change in lamellar repeat and layer thicknesses with composition: $d(d_{001})/d\phi_{PS}$, $dl_{PS}/d\phi_{PS}$, and $dl_{PI}/d\phi_{PS}$. Examination of Fig. 6 shows that for the hPS blends, the increase in l_{PS} more than offsets the corresponding decrease in l_{PI} so that the overall lamellar repeat spacing increases with hPS content. Average values of $d(d_{001})/d\phi_{PS}$, $dl_{PS}/d\phi_{PS}$, and $dl_{PI}/d\phi_{PS}$ are shown in Table 3. The rate of increase in the PS layer by swelling is about 2.5 × that of the rate of decrease in the PI layer due to the spreading apart of the junction points on the IMDS due to addition of homopolymer. On the other hand, for the addition of hPI, the rate of increase of the PI layer is only about 1.1 × than the decrease rate of the PS layer so that in the hPI blends the overall d-spacing is approximately constant. In this case the addition of homopolymer into the domains with *interior* junctions causes greater lateral swelling than axial swelling, presumably to relieve overcrowding. The 3DB and SH polymers show a somewhat greater effect than the 2DB, consistent with the higher junction functionality in these materials. In the 2DB and 3DB there are a total of 2 and 3 PI blocks, respectively constricted by 3- and 4-junction points. The small increase in d-spacing and the dramatic increase in σ also indicate that bridges of the PI chains maybe more numerous than loops leading to a restriction on the PI axial swelling. The structure remains lamellar even to very large compositional asymmetry (20% PS:80% PI) suggesting that the PI chains prefer to bridge across a flat interface with constant width instead across the curved IMDS of cylinders of variable width.

The lamellar-catenoid morphology in binary blends of a PS-*b*-PB diblock can be understood by comparing the double diamond structure observed by Winey et al. [34] on binary blends of either PS-*b*-PI and hP or PS-*b*-PB and hPS with approximately the same molecular weight and the same overall volume fraction of PS ($\phi_{PS} = 0.65$–0.67). The TEM (Fig. 3f) and SAXS (Fig. 5a) data show a structure that is lamellar to first order but is modified by channels in the PI layers that are apparently catenoidal in shape. SAXS of such a sample gives peaks with a q_n/q_1 ratio corresponding to lamellar morphologies.

A theoretical study made by Fredrickson [40] examined the stability of such a LC phase in the strong segregation limit, which is the regime that our binary blend belongs to, and predicts that the LC morphology is not the most favorable structure. Olvera de la Cruz et al. [41] showed that in the weak segregation regime a structure similar to the LC occurs when ϕ_A is near to 0.5, even though lamellae are expected in such composition. Zhu et al. have provided a more detailed structural analysis for the LC phase [42]. Recently Gido et al. [43] studied the phase behavior of I_2S single graft block copolymers/homopolymer blends and observed a hexagonally perforated lamellar morphology (HPL) similar to the LC structure exhibited here.

The behavior of the SH-20/20 blends is different from the

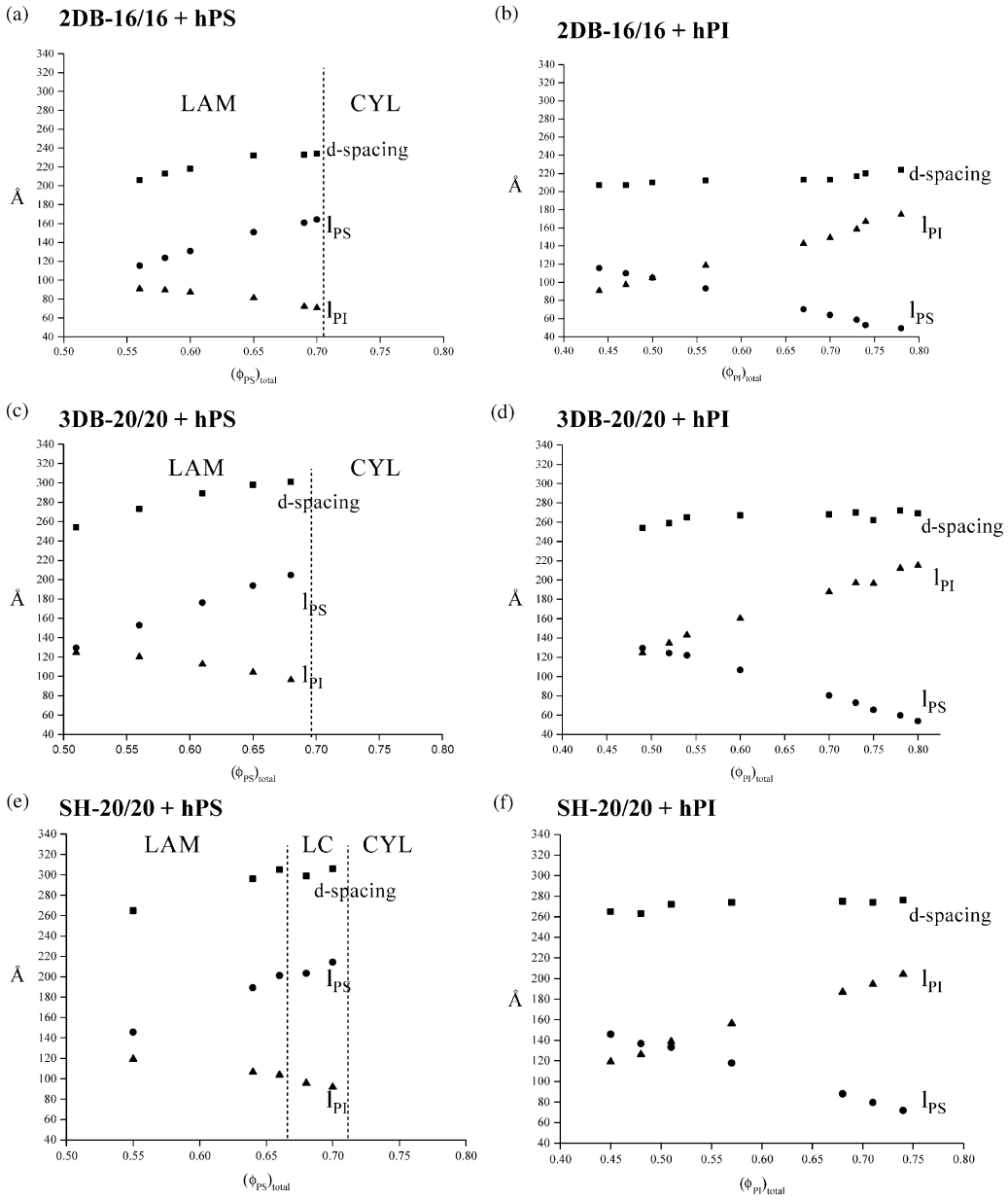

Fig. 6. Lamellar repeat and individual PS and PI layer versus total volume fraction of PS and PI in the neat copolymers and their blends. (a) 2DB-16/16 + hPS, (b) 2DB-16/16 + hPI, (c) 3DB-20/20 + hPS, (d) 3DB-20/20 + hPI, (e) SH-20/20 + hPS and (f) SH-20/20 + hPI.

3DB-20/20 blends because the Super H-shaped copolymer molecule is symmetric. The behavior upon swelling with hPS shows the appearance of the LC structure only in the SH blends. According to Gido et al. [20] a formal division of H-shaped molecular architectures can be considered in order to map the morphological behavior of such complex systems onto the simple graft (A_nB, symmetric and non-symmetric cases) morphology diagram. In our case the behavior is different for two reasons:

(i) The architecture of a super H-shaped molecule leads to a complex structure when it is divided (the 3DB-20/20 sample) and
(ii) The arms which are linked to the difunctional living end are not simple homopolymer chains but are *diblock* chains leading to a large increase in the number of junctions (8 in our case compared to just 2 for the H-shaped sample in Ref. [20]). The half molecule, $(AB)_3A$, therefore does not behave as the simple A_2B polymer as in the case of the division of the H architecture (A_2BA_2).

5. Conclusions

The neat 2DB, 3DB and SH miktoarm star block copolymers exhibited a lamellar microdomain structure. These complex molecules were then blended with hPS or hPI. A

transition from lamellar to hexagonally packed PI cylinders was induced via hPS swelling in all samples without the observation of an intervening cubic structure. Swelling with hPI retained the lamellar microdomain morphology for all the samples up to $(\phi_{PI})_{total} = 0.80$. Only in the case of hPS swelling of the SH sample, did an intermediate LC structure occur between the lamellar and the cylindrical microstructures. The changes in area per junction, layer thickness and lamellar repeat with addition of homopolymer showed strong differences between swelling the exterior PS blocks vs. the interior PI blocks.

Acknowledgements

The authors acknowledge Dr Malcom Capel for his technical assistance at the National Synchrotron Light Source at Brookhaven National Laboratory and Dr Ramon Albalak for his help in the X-ray facility located at MIT. We also thank Dr Lars Kielhorn and Prof. Murugappan Muthukumar from the University of Massachusetts at Amherst for the theoretical calculations of the $(\chi N)_{spinodal}$. This project was supported by ACS PRF No. 30050-AC7, AFOSR ASSERT No. F49 620-94-1-0357 and NSF-DMR 9705271. A.A and N.H. acknowledge the Greek General Secreteriat of Research and Technology and the Research Committee of the University of Athens for financial support.

References

[1] Roe R-J, Zin W-C. Macromolecules 1984;17:189.
[2] Nojima S, Roe R-J. Macromolecules 1987;20:1866.
[3] Owens JN, Gancarz IS, Koberstein JT, Russell TP. Macromolecules 1989;22:3388.
[4] Inoue T, Moritani M, Hashimoto T, Kawai H. Macromolecules 1971;4:500.
[5] Cohen RE, Wilfong DE. Macromolecules 1982;15:370.
[6] Bates FS, Cohen RE, Argon AS. Macromolecules 1983;16:1108.
[7] Watanabe H, Kotaka T. Macromolecules 1983;16:769.
[8] Watanabe H, Kotaka T. Macromolecules 1984;17:342.
[9] Berney CV, Cheng P-L, Cohen RE. Macromolecules 1988;21:2235.
[10] Cheng P-L, Berney CV, Cohen RE. Makromol Chem 1989;190:589.
[11] Kinning DJ, Thomas EL, Fetters LJ. J Chem Phys 1989;90:5806.
[12] Hashimoto T, Tanaka H, Hasegawa H. Macromolecules 1990;23:4378.
[13] Tanaka H, Hasegawa H, Hashimoto T. Macromolecules 1991;24:240.
[14] Winey KI, Thomas EL, Fetters LJ. J Chem Phys 1991;95(12):9367.
[15] Milner ST. Macromolecules 1994;27:2335.
[16] Olmsted PD, Milner ST. Macromolecules 1998;31:4011.
[17] Hadjichristidis N, Iatrou H, Behal SK, Chludzinski JJ, Disko MM, Garner RT, Liang KS, Lohse DJ, Milner ST. Macromolecules 1993;26:5812.
[18] Matsushita Y, Noda I. Macromol Symp 1996;106:251.
[19] Pochan DJ, Gido SP, Pispas S, Mays JW, Ryan AJ, Fairclough PA, Hamley IW, Terrrill N. Macromolecules 1996;29:5091.
[20] Gido SP, Pochan DJ, Pispas S, Mays JW, Hadjichristidis N. Macromolecules 1996;29:7022.
[21] Tselikas Y, Iatrou H, Hadjichristidis N, Liang KS, Lohse DJ. J Chem Phys 1996;105(6):2456.
[22] Beyer FL, Gido SP, Velis G, Hadjichristidis N, Beck Tan N. Macromolecules 1999;32:6604.
[23] Beyer FL, Gido SP, Poulos Y, Avgeropoulos A, Hadjichristidis N. Macromolecules 1997;30:2373.
[24] Beyer FL, Gido SP, Uhrig D, Mays JW, Beck Tan N, Trevino SF. J Polym Sci, Part B: Polym Phys 1999;37:3392.
[25] Turner CM, Sheller NB, Foster MD, Lee B, Corona-Galvin S, Quirk RP, Annis B, Lin J-S. Macromolecules 1998;31:4372.
[26] Lee C, Gido SP, Poulos Y, Hadjichristidis N, Beck Tan N, Trevino SF, Mays JW. Polymer 1998;39:4631.
[27] Lee C, Gido SP, Poulos Y, Hadjichristidis N, Beck Tan N, Trevino SF, Mays JW. J Chem Phys 1997;107:6460.
[28] Xenidou M, Beyer FL, Gido SP, Hadjichristidis N, Beck Tan N. Macromolecules 1998;31:7659.
[29] Tselikas Y, Hadjichristidis N, Lescanec RL, Honeker CC, Wohlgemuth M, Thomas EL. Macromolecules 1996;29:3390.
[30] Avgeropoulos A, Hadjichristidis N. J Polym Sci A: Polym Chem 1997;35:813.
[31] Kielhorn L, Muthukumar M. Personal communication.
[32] Brandrup J, Immergut EH. Polymer handbook. 3rd ed. Wiley, 1989.
[33] Winey KI, Thomas EL, Fetters LJ. Macromolecules 1991;24:6182.
[34] Winey KI, Thomas EL, Fetters LJ. Macromolecules 1992;25:422.
[35] Avgeropoulos A, Dair BJ, Hadjichristidis N, Thomas EL. Macromolecules 1997;30:5634.
[36] Laurer JH, Hajduk DA, Fung JC, Sedat JW, Smith SD, Gruner SM, Agard DA, Spontak RJ. Macromolecules 1997;30:3938.
[37] Disko MM, Liang KS, Behal SK, Roe RJ, Jeon KJ. Macromolecules 1993;26:2983.
[38] Thomas EL, Anderson DM, Henkee CS, Hoffman D. Nature 1988;334:598.
[39] Seddon JM. Biophys Acta 1990;1031:1.
[40] Fredrickson GH. Macromolecules 1991;24:3456.
[41] Olvera de la Cruz M, Mayes AM, Swift BW. Macromolecules 1992;25:944.
[42] Zhu L, Huang P, Cheng SZD, Ge Q, Quirk RP, Thomas EL, Lotz B, Wittmann J-C, Hsiao BS, Yeh F, Liu L. Phys Rev Lett 2001;86:6030.
[43] Yang L, Gido SP, Mays JW, Pispas S, Hadjichristidis N. Macromolecules 2001;34:4235.
[44] Mori K, Hasegawa H, Hashimoto T. Polym J 1985;17:799.
[45] Wolff T, Burger C, Ruland W. Macromolecules 1993;26:1707.